T_2 Relaxometry with Indirect Echo Compensation from Highly Undersampled Data

Chuan Huang[1,2], **Ali Bilgin**[3,4], **Tomoe Barr**[4], and **Maria I. Altbach**[5,*]

[1]Department of Mathematics, University of Arizona, Tucson, Arizona, USA

[2]Center for Advanced Radiological Sciences, Massachusetts General Hospital, Boston, Massachusetts, USA

[3]Department of Electrical and Computer Engineering, University of Arizona, Tucson, Arizona, USA

[4]Department of Biomedical Engineering, University of Arizona, Tucson, Arizona, USA

[5]Department of Medical Imaging, University of Arizona, Tucson, Arizona, USA

Abstract

Purpose—To develop an algorithm for fast and accurate T_2 estimation from highly undersampled multi-echo spin-echo (MESE) data.

Methods—The algorithm combines a model-based reconstruction with a signal decay based on the slice-resolved extended phase graph (SEPG) model with the goal of reconstructing T_2 maps from highly undersampled radial MESE data with indirect echo compensation. To avoid problems associated with the nonlinearity of the SEPG model, principal component decomposition is used to linearize the signal model. The proposed *CUrve Reconstruction via pca-based Linearization with Indirect Echo compensation (CURLIE)* algorithm is used to estimate T_2 curves from highly undersampled data. T_2 maps are obtained by fitting the curves to the SEPG model.

Results—Results on phantoms showed T_2 biases (1.9% to 18.4%) when indirect echoes are not taken into account. The T_2 biases were reduced (<3.2%) when the CURLIE reconstruction was performed along with SEPG fitting even for high degrees of undersampling (4% sampled). Experiments in vivo for brain, liver and heart followed the same trend as the phantoms.

Conclusion—The CURLIE reconstruction combined with SEPG fitting enables accurate T_2 estimation from highly undersampled MESE radial data thus, yielding a fast T_2 mapping method without errors caused by indirect echoes.

Keywords

T_2 estimation; relaxometry; FSE; stimulated echo; indirect echo; principal component analysis; non-180° refocusing pulse

Introduction

Spin-spin (T_2) relaxation is one of the main contrast mechanisms in MRI. Although most clinical applications use qualitative (visual) information derived from T_2-weighted images, there is an increasing interest in T_2 mapping (1–10).

*Correspondence should be addressed to: Maria I. Altbach, PhD, Department of Medical Imaging, University of Arizona, Tucson, AZ 85724, Phone: (520) 626–5532, Fax: (520) 621–8522, maltbach@email.arizona.edu.

Because single-echo spin-echo T_2 mapping requires long acquisition times, its translation to the clinic has been limited by its time inefficiency. In order to reduce the acquisition times it is customary to use multi-echo spin-echo (MESE) pulse sequences, where several echo time (TE) points are acquired per repetition time (TR) period by using a train of 180° refocusing pulses after the initial 90° excitation pulse. To further accelerate T_2 data acquisition a fast (or turbo) spin-echo approach where several k-space lines of data are acquired per TR period is commonly used. For the sake of speed in T_2 mapping (while maintaining high spatial and temporal resolution), the use of TE data sets that are undersampled in k-space has been proposed in conjunction with a fast spin-echo approach. Several algorithms have been described to recover T_2 information from these highly reduced TE data sets (11–16). Recently, the focus has been on model-based T_2 mapping algorithms. Doneva et al. proposed to exploit the temporal sparsity of the exponential decay while reconstructing all TE images under the framework of compressed sensing (13, 16). Block et al. proposed a model-based algorithm for radial fast spin-echo acquisitions to directly reconstruct I_0 and R_2 ($1/T_2$) maps from the measured k-space data (11). Because I_0 and R_2 values have very different scales the gradient-based minimization process requires a scaling factor which needs to be fine tuned for accurate T_2 estimation (12). Our group has recently developed the REPCOM (REconstruction of Principal COmponent coefficient Maps) algorithm which linearizes the signal model using principal component analysis (PCA). REPCOM exploits the spatial and temporal sparsity of the TE images, and provides accurate T_2 estimates from highly undersampled data without the need of a scaling factor for the fitted parameters.

The algorithms described above, including REPCOM, rely on the assumption that the signal follows an exponential decay. However, in MESE acquisitions the decay is generally contaminated by indirect echoes (echoes leading to signal generation after more than one refocusing pulse such as stimulated echoes) including differences in the signal intensities between even and odd echoes, thus, altering the single exponential nature of the T_2 decay observed in a single-echo spin-echo experiment. The indirect echoes are the result of refocusing pulses not attaining the ideal 180° flip angle (FA) due to nonrectangular slice profiles, static (B_0) and transmit field (B_1) inhomogeneity, and B_1 calibration errors (17).

To alleviate the pulse imperfection due to nonrectangular slice profiles, a thick refocusing slice technique has been proposed by Pell et al. (5). This technique employs a refocusing slice that is thicker than the excitation slice. B_0 and B_1 inhomogeneity, and calibration errors, however, are not corrected for by this approach. Echo editing techniques that use crusher gradients around the refocusing pulses have also been proposed to reduce the signal resulting from pathways leading to indirect echoes (18–20). However, not all pathways can be crushed effectively and the method has only been demonstrated with non-selective refocusing pulses, which limits the use of the method to single slice applications. Recently, Lebel and Wilman proposed the slice-resolved extended phase graph (SEPG) fitting algorithm (17), for accurate T_2 estimation from MESE data contaminated by indirect echoes. Their method is based on the extended phase graph (EPG) model proposed by Hennig (21) which provides decay curves for any given refocusing FA. The EPG model assumes perfectly rectangular slice profiles whereas the SEPG model includes the known slice profile for both excitation and refocusing pulses. The fitting algorithm fits the measurements to the SEPG model to obtain the T_2 estimates. The method is robust to B_1 inhomogeneity and calibration errors and it has been shown that accurate T_2 estimation can be obtained from MESE data acquired with reduced FAs (<180°).

So far, the SEPG fitting algorithm has been demonstrated for fully sampled or 60% partial k-space Cartesian data. The main limitation of combining the SEPG fitting algorithm with a model-based reconstruction approach for T_2 estimation from highly undersampled data (< 10% sampled with respect to Nyquist sampling theorem), is the non-linearity of the SEPG

model. In this work we propose to extend the PCA approach used in the REPCOM algorithm to linearize the SEPG model. The proposed *CUrve Reconstruction via pca based Linearization with Indirect Echo compensation* (CURLIE) algorithm aims to obtain accurate T_2 decay curves from highly undersampled data in the presence of B_1 imperfections or non-180° refocusing pulses. The T_2 values of the reconstructed curves can then be obtained by applying SEPG fitting. Although only radial data is used in this work, the methodology can be translated to other trajectories.

Theory

Hennig's EPG model provides a way to calculate the signal intensity of a specific echo point for MESE sequences with the assumption that all spins experience the same FA. Given the excitation pulse FA, α_0, the FAs of the N refocusing pulses, α_j (j=1, … N), the sensitivity of transmit B_1 field, and the I_0, T_1 and T_2 values of a voxel, the signal intensity at the jth spin echo, S_j, can be expressed as according to ref.21:

$$S_j = I_0 \cdot EPG(T_1, T_2, B_1, \alpha_0, \ldots, \alpha_j, j). \quad [1]$$

The function $EPG(\bullet)$ does not have an explicit expression, but can be computed numerically. Based on the EPG model, Lebel and Wilman recently proposed the SEPG model. With the prior knowledge of the prescribed slice profile of the excitation pulse along the z direction, $\alpha_0(z)$, the prescribed slice profiles of the refocusing pulse along the z direction, $\alpha_j(z)$ (j=1, …, N), the SEPG model can be obtained by integrating the EPG model throughout the slice:

$$C_j(I_0, T_1, T_2, B_1, \alpha_0(z), \ldots, \alpha_j(z)) = I_0 \cdot \int_z EPG(T_1, T_2, B_1, \alpha_0(z), \ldots, \alpha_j(z), j)dz. \quad [2]$$

The SEPG fitting algorithm fits T_2 decay curves acquired with a MESE sequence to Equation [2]. Given N TE measurements s_j (j=1, …, N), the SEPG fitting algorithm can be written as:

$$I_0, T_1, T_2, B_1 = \arg\min_{I_0, T_1, T_2, B_1} \{\sum_{j=1}^{N} \| C_j(I_0, T_1, T_2, B_1, \alpha_0(z), \ldots, \alpha_j(z)) - s_j \|^2\}. \quad [3]$$

In Ref. 17, it has been shown that the SEPG model is insensitive to T_1 values when T_1/T_2 ratio is large, hence it has been proposed to fix T_1 to $+\infty$ in order to simplify the signal model and the fitting algorithm:

$$C'(I_0, T_2, B_1, \alpha_0(z), \ldots, \alpha_j(z), j) = I_0 \cdot \int_z EPG(T_1 = +\infty, T_2, B_1, \alpha_0(z), \ldots, \alpha_j(z), j)dz, \quad [4]$$

$$I_0, T_2, B_1 = \arg\min_{I_0, T_2, B_1} \{\sum_{j=1}^{N} \| C_j'(I_0, T_1 = +\infty, T_2, B_1, \alpha_0(z), \ldots, \alpha_j(z)) - s_j \|^2\}. \quad [5]$$

In the published work of the SEPG fitting algorithm, the amplitude images were obtained from fully or 60% sampled Cartesian k-space. For highly undersampled data (< 10% sampled), the fitting algorithm relies on a reconstruction algorithm which can accurately recover the decay curves. Thus, it is intuitive to combine the SEPG model with a model-based algorithm (11, 22):

$$\mathbf{I}_0, \mathbf{T}_2, \mathbf{B}_1 = \arg\min_{\mathbf{I}_0,\mathbf{T}_2,\mathbf{B}_1} \{\sum_{j=1}^{N} \| FT\{C_j{}'(I_0, T_1, T_2, B_1, \alpha_0(z), \ldots, \alpha_j(z))\} - \mathbf{K}_j \|^2\}, \quad [6]$$

where $\mathbf{I}_0$,$\mathbf{T}_2$,$\mathbf{B}_1$ are the vectors of I_0, T_2, B_1 of all voxels, FT is the forward Fourier transform, $\mathbf{K}_j$ is the (undersampled) k-space data acquired at the j^{th} TE. Due to the large dimensionality of the problem, it is impractical to use a global minimization algorithm to solve Equation [6], hence a local minimization algorithm (such as the gradient-based minimization algorithm) can be used. However, the SEPG model is non-linear as a function of T_2 and B_1 and it is difficult to obtain the gradient for minimization purposes.

In the REPCOM algorithm (12), we use PCA to linearize the exponential T_2 decay model, thus overcoming non-linear minimization problems. In CURLIE we extend the PCA approach to approximate the SEPG model. The principal components (PCs) are calculated for given TE points using a training set of decay curves given by the SEPG model for a certain range of T_2 and B_1 values. With the PCs obtained from the training curves, the T_2 decay curves with indirect echoes can be approximated by a weighted linear combination of the PCs.

Let $\vec{v}$ be a vector representing a noiseless T_2 decay curve with indirect echoes. Let L be the number of PCs to be used in the approximation and $\vec{p_i}$ the ith PC vector. $\vec{v}$ can be approximated by a linear combination of $\vec{p_i}$:

$$\vec{v} = \sum_{i=1}^{L} m_i \vec{p}_i, \quad [7]$$

where m_i is the weighting of the ith principal component. $\hat{\mathbf{P}} = (\vec{p_1}, \vec{p_2}, \ldots, \vec{p_L})$ is the matrix consisting of the vectors of the first L PCs. Let $\vec{M_i}$ be the vector of m_i for all the voxels and $\mathbf{M}$ can be formed as $(\vec{M_1}, \vec{M_2}, \ldots, \vec{M_L})$. Let $\hat{\mathbf{P}}_j$ denote the jth row of the matrix $\hat{\mathbf{P}}$. Note that $\mathbf{M}\hat{\mathbf{P}}_j^T$ yields the image at TE_j from the L principal component coefficients. Equation [6] can be reformulated as:

$$\widehat{\mathbf{M}} = \arg\min_{\mathbf{M}} \{\sum_{j=1}^{L} \left| |FT_j(\mathbf{M}\hat{\mathbf{P}}_j^T) - \vec{\mathbf{K}}_j| \right|^2\}. \quad [8]$$

When the complex coil sensitivity profiles $\mathbf{S}_l$ and the sparsifying penalties $Penalty_i(\cdot)$ (with corresponding weights λ_i) are given (12), the algorithm can be written as:

$$\widehat{\mathbf{M}} = \arg\min_{\mathbf{M}} \{\sum_{l=1}^{\#coils} \sum_{j=1}^{L} \left| |FT_j(\mathbf{S}_l\mathbf{M}\hat{\mathbf{P}}_j^T) - \vec{\mathbf{K}}_{l,j}| \right|^2 + \sum_i \lambda_i Penalty_i(\mathbf{M})\}. \quad [9]$$

The penalty terms are used to exploit the spatial compressibility of the PC coefficient maps in the framework of compressed sensing and have been shown to improve the quality of the reconstructed T_2 maps (12). The decay curves are reconstructed from $\hat{\mathbf{M}}$ which can be obtained by a conjugate gradient minimization algorithm.

The SEPG fitting algorithm (Equation [5]) can then be applied to the curves reconstructed by CURLIE to obtain T_2 estimates. As mentioned above, Lebel and Wilman proposed to fix the T_1 to be $+\infty$ for the fitting (17). As an alternative, an optimized T_1 value can be used in the SEPG fitting based on the prior knowledge of the anatomy being imaged as indicated by Sénégas et al. (23).

The flow chart of the CURLIE reconstruction algorithm and the SEPG fitting is shown in Figure 1. Different from REPCOM, the new method includes the effects of indirect echoes in the T_2 estimation process by incorporating the SEPG model in the generation of the training curves and in the estimation of the principal components coefficients (via the CURLIE algorithm) as well as in the fitting of the TE images to obtain the final T_2 map.

Methods

All radial MESE data were acquired on a 1.5T Signa HDxt GE (General Electric Healthcare, Milwaukee, WI) MR scanner using a previously developed radial fast spin-echo (radFSE) pulse sequence (24). A "bit-reversed" angular ordering was used to minimize artifacts from T_2 decay and motion (25). The slice profiles of the excitation and refocusing pulses were generated from the Fourier transform of the RF waveforms provided by the manufacturer for fast spin-echo pulse sequences. The refocusing slice RF profiles are calibrated by the techniques in Ref. 26. It should be noted that in the manufacturer's pulse sequence the full-width half-maximum of the refocusing pulses is designed to be about 1.6 times as thick as the corresponding excitation pulse.

Computer simulation

Curves were generated according to the SEPG model assuming an ETL = 16 and echo spacing =12.11 ms with the slice discretized into 63 points along the slice profile. A total of 765 curves were generated for T_2 values varying from 50 ms to 300 ms with a step size of 5 ms, B_1 values varying from 0.5 to 1.2 with a step size of 0.05, and $T_1 = +\infty$. The PCs were trained from these 765 curves.

Phantom Data

A physical phantom, containing three 10 mm glass tubes filled with $MnCl_2$ solutions of different concentrations (50 μM, 75 μM, and 170 μM) to yield data at different T_2's, was prepared. RadFSE data were acquired with a single channel transmit/receive coil, with an echo train length (ETL) of 16 with echo points spaced by 12.11 ms, TR = 1 s, excitation slice thickness = 8 mm, receiver bandwidth = ±15.63 kHz, field of view (FOV) = 10 cm. The acquisition matrix for undersampled data was 256×256 yielding 16 radial k-space lines for each of the 16 TE data sets. For comparison purposes, another data set was acquired with an acquisition matrix of 256×4096 to yield 256 radial k-space lines for each TE; all other acquisition parameters were kept the same. Although for radial acquisition a data set with 256 radial lines and 256 sampling points per line is 64% sampled (according to the Nyquist theorem a fully sampled data set requires 402 radial lines for 256 sampling points per line), the data set gives good quality images and accurate T_2 maps for most clinical applications (as well as for our phantom work). In this work, this data set is referred to as "standard sampled".

Cartesian single-echo spin-echo data (not contaminated by indirect echoes) of the phantom were also acquired to obtain the gold standard T_2 values. Data were acquired with a single channel transmit/receive coil, TR = 5 s, excitation slice thickness = 8 mm with the refocusing slice being approximately 5 times as thick as the excitation slice, receiver bandwidth = ±15.63 kHz, and FOV = 10 cm. Data for 4 TE points (12, 24, 36 and 48 ms) were acquired with the acquisition matrix per TE point set to 64×64. A lower resolution was used for the single-echo spin-echo sequence due to its long acquisition time. Gold standard T_2 values were obtained by fitting the data to a single exponential decay.

In vivo data

Each in vivo data set (brain, liver and heart) were acquired from a separate volunteer under informed consent with a protocol approved by the local Institutional Review Board.

In vivo brain data were acquired using the radFSE pulse sequence with an 8-channel receiver head coil, 16 TE points equispaced by 12.93 ms, excitation slice thickness = 8 mm, receiver bandwidth = ±15.63 kHz, TR = 4 s, and FOV = 24 cm. The acquisition matrix for the standard sampled data set was 256×4096 to yield 256 radial lines per TE. The acquisition matrix for the undersampled data set was 256×512 yielding 32 radial lines per TE (8.0% sampled compared to fully sampled data). Experiments were conducted with the refocusing RF pulses FAs prescribed to be 180° and 120°.

In vivo liver data were acquired in a breath hold using the radFSE pulse sequence with an 8-channel receiver torso coil, 16 TE points equispaced by 8.93 ms, slice thickness = 8 mm, receiver bandwidth = ±31.25 kHz, TR = 1.5 s, FOV = 48 cm, and acquisition matrix = 256×256 to yield 16 radial lines per TE (4.0% sampled compared to fully sampled data). To evaluate the estimated T_2 values, three tubes containing either $MnCl_2$ or agarose for T_2 variation were placed on the subject's chest. The gold standard T_2 values of the three tubes were estimated to be 56.0 ms, 77.9 ms and 64.0 ms in a separate experiment using a single-echo spin-echo sequence.

In vivo cardiac data were acquired using a radFSE pulse sequence which included a double-inversion preparation period for nulling the signal from flowing blood (27). Data were acquired with an 8-channel receiver cardiac coil, 16 TE points equispaced by 9.46 ms (for refocusing pulses with prescribed FA=180°) or 6.85 ms (for refocusing pulses with prescribed FA=155°), slice thickness = 8 mm, receiver bandwidth = ±31.25 kHz, TR = 1 RR, and FOV = 48 cm. The acquisition matrix was 256×256 resulting in 16 radial lines per TE (4.0 % sampled compared to fully sampled data). Imaging of a slice was completed within a breath hold (~ 15–18 s).

Data Reconstruction

All algorithms were implemented in Matlab (MathWorks, Natick, MA). The training curves for PC ($\hat{\mathbf{P}}$) generation were provided by the SEPG signal model using Equation [3]. Equation [8] was solved iteratively by using the nonlinear Polak-Ribiere Conjugate Gradient algorithm (28). The spatial penalty terms used in Equation [9] consisted of the 1-norms of the wavelet transform (Daubechies 4, code obtained from http://www-stat.stanford.edu/~wavelab) and total variation of the PC coefficient maps.

T_2 estimates were obtained either by conventional exponential fitting or by SEPG fitting. SEPG fitting was performed using Equation [4]; during the fitting, T_2 was allowed to vary between 30 – 5000 ms and B_1 was limited to 0 – 3. The T_1 values used in the SEPG fitting were fixed to an optimal value using prior information. For each in vivo image a single T_1 was chosen based on reported values for the anatomy of interest: gray matter for brain (950 ms) (29), liver (500 ms) (30) and myocardium (700 ms) (31). For the phantom data, where there was a wide range of T_1 values among the different vials used, the optimal T_1 was determined as proposed in Ref. 23. In brief, a set of simulated curves were generated using the SEPG model with T_1, T_2, and B_1 varying independently between 300~2000 ms, 50~300 ms, and 0.5~1.2, respectively. SEPG fitting was then performed on these curves for each of the T_1 values in the selected range. The T_1 value that minimized the T_2 estimation error according to the 2-norm was selected to be the optimized T_1.

For comparison, T_2 maps were also reconstructed using the REPCOM algorithm. The T_2 values for the PC training were between 35 ms to 300 ms equi-spaced by 1 ms. Total

variation and wavelet transforms were used as the sparsifying transform with proper weightings as in Ref. 12.

Results

Proof-of-Concept

In order to demonstrate that a small number of PCs are sufficient to characterize the T_2 decay curves in the presence of indirect echoes, we first performed simulations. Figure 2a shows 4 out of the 765 curves generated according to the SEPG model. The curves show the expected signal modulation due to indirect echoes with modulations increasing with B_1. Figure 2b shows the 2-norm of the approximation error when 6 PCs are used to represent the curves after these are normalized so that the 2-norm is unity. Note that the 2-norms of the approximation error are all below 0.006 and most of the errors have 2-norm < 0.003. Figure 2c shows the distribution of the % error of the T_2 values estimated by SEPG fitting caused by the PC approximation. As shown, the % errors in T_2 values estimated from the curves recovered from 6 PCs are all < 3.5% with majority of the errors being < 1.5%. These experiments show that it is sufficient to use $L = 6$ to represent the training curves accurately under the given conditions and that the approximation error caused by using only the first 6 PCs is small.

Experiments using physical phantom data were performed to further investigate the accuracy of the linear approximation using principal component decomposition. Phantom data were acquired with radFSE using standard sampled data (256 radial lines per TE with 256 points per radial line). Figure 3a–d show decay curves reconstructed directly from the acquired data for each of the three phantom tubes shown in the image and for various refocusing FA. Each point in the decay curves corresponds to the averaged signal from voxels within an ROI for each tube; each curve is the fitted decay curve according to the SEPG model from fitting parameters using the SEPG fitting ($T_1 = +\infty$). The curves are normalized (2-norm=1). As shown, the fitted curves are well matched to the acquired data for all the four FAs. Figure 3e–g show the approximation error of the corresponding curves recovered from the 6 PCs used to generate Figure 2b–c. The errors are all below 0.01 with most under 0.005. The 2-norms of the approximation error are between 0.0018 and 0.0042 for all FAs which also show that 6 PCs can represent the decay curves of the acquired data well. Note that the same PCs were used for all FAs (FA changes are equivalent to B_1 changes under the model). In this experiment T_1 was not optimized and assumed to be $+\infty$.

We then evaluated the accuracy of T_2 estimation using the curves recovered from 6 PCs using the standard sampled phantom data. Table 1 compares the bias in T_2 estimates obtained from the “recovered curves” to those from curves obtained directly from the TE images (“original curves”). The table shows results for various FA and for three fitting algorithms: exponential fitting, SEPG fitting with $T_1 = +\infty$, and SEPG fitting with T_1 optimized. It can be observed that for each fitting algorithm the bias of T_2 estimates obtained from the original and recovered curves are very similar. The differences in T_2 bias are all below 0.3%, which further demonstrates the accuracy of the PC approximation for representing the acquired decay curves. The results also show that the exponential fitting of MESE data overestimates T_2 values. The estimation bias increases as T_2 increases and as the FA diverges from 180° due to the more pronounced indirect echo effect; for FA = 120°, the bias of the exponential fitting can be up to 18.4% (with the larger bias for T_2=210 ms). The bias of the SEPG fitting with $T_1 = +\infty$ is less than 6% which is significantly smaller than the bias of the exponential fitting. When an optimized T_1 (500 ms) was used, the largest error is further reduced to 3.6% which demonstrates that the optimized T_1 can be used in the SEPG fitting to improve T_2 estimation.

T_2 estimation from highly undersampled data

So far, we have demonstrated that a few principal components can accurately represent the T_2 decay curves contaminated with indirect echoes using standard sampled data. For highly undersampled data we need to use the CURLIE algorithm described in Equation [8], where the PCA-based signal model is used to match the acquired k-space data. Using the three-tube physical phantom and highly undersampled radFSE data (i.e., data with only 16 radial lines per TE) we tested the accuracy of CURLIE for reconstructing the decay curves using 6 PCs. Figure 4 shows the difference between curves reconstructed from highly undersampled data using CURLIE and curves obtained from the standard sampled data (64% sampled) for various FAs. In general, the differences between the curves are small despite the fact that the highly undersampled data has 16 times less samples than the standard sampled data. The 2-norms of the differences are between 0.0035 and 0.0095 which demonstrates that decay curves from highly undersampled data can be accurately reconstructed by CURLIE. The T_2 estimates for the three tubes in the phantom, obtained with SEPG fitting, are shown in Table 2. Note that the T_2 bias of undersampled data is similar to the T_2 bias obtained for standard sampled data (data from Table 1): less than 5% for $T_1 = +\infty$ and less than 3.6% for $T_1 = 500$ ms. This demonstrates that the decay curves reconstructed by CURLIE from highly undersampled data have the same T_2 characteristics as the decay curves obtained from the standard sampled data.

CURLIE was tested in vivo using brain data. Two experiments were conducted: one where the prescribed FA of the refocusing pulses was 180°, another where the prescribed FA was 120°. The same 6 PCs used in Table 2 were used for the reconstruction of the undersampled brain data. In Figure 5, the decay curves of the shown ROI obtained from standard sampled data (directly from the TE images) are compared to the curves reconstructed from 32 radial lines per TE (8.0% sampled) using CURLIE. Note that the curves generated from under- and standard sampled data are very similar (the error for all echo points for each of the two FA are below 0.01). The T_2 values obtained from the decay curves using SEPG fitting are also shown in the figure. The differences between the T_2 values obtained from under- and standard sampled data are below 3%. These results show that the curves reconstructed from highly undersampled in vivo data agree well with the decay curves obtained from standard sampled data. Also, note that the T_2 values estimated from data acquired with 180° and 120° FAs are similar.

A voxel-wise brain T_2 map obtained using CURLIE and SEPG fitting for data acquired with prescribed FAs of 180° is shown in Figure 6a. Figure 6b shows the difference map between data acquired with prescribed FAs of 180° and 120° but reconstructed with the REPCOM algorithm (i.e. where the training curves do not take into account indirect echoes and single exponential fitting is used for T_2 estimation). The % difference maps between T_2 maps obtained by CURLIE with SEPG fitting from data acquired with prescribed FAs of 180° and 120° is shown in Figure 6c and 6d for T_1=+∞ and T_1=950 ms, respectively. The same 6 PCs as in previous figures were used for both FAs. In the % difference maps, the ventricles are masked out due to the fact that the T_2 of cerebrospinal fluid (~ 2000 ms) is much larger than the white and gray matter, and the TE coverage used here is not suitable for the accurate estimation of long T_2s. The means of the difference map are: 8.3% for the map derived from the REPCOM reconstruction and 4.9% and 3.1% for the maps derived from CURLIE and SEPG fitting with $T_1 = +\infty$ and $T_1 = 950$ ms, respectively. The small means in the difference maps support the concept that the CURLIE reconstruction followed by SEPG fitting significantly reduces the effect of indirect echoes in T_2 estimation in vivo. When an optimized T_1 is used in the SEPG fitting the % difference T_2 map obtained by SEPG fitting with optimized T_1 is generally smaller. It is noteworthy to point out that since the data sets with 180° and 120° FAs were obtained by two separate acquisitions, there is slight

difference between the two imaging slices due to inter-scan movement even though the same slice was prescribed.

We also investigated the utility of T_2 mapping with CURLIE and SEPG fitting for abdominal imaging where high undersampling is needed due to the acquisition time constraint imposed by the breath hold. Figure 7 shows the anatomical images and the voxel-wise T_2 maps of an abdominal slice. The maps were reconstructed from highly undersampled data (16 radial k-space lines per TE; 4.0% sampled) by REPCOM and CURLIE with optimized T_1 SEPG fitting. Three phantoms with known T_2 values were placed above the subject during data acquisition and used as the gold standard (due to the breath hold limitation, it was not possible to obtain a gold standard data set for the liver T_2 map). The CURLIE reconstructions were performed with $L = 6$. The PCs were obtained from training curves generated for a T_2 range of 35 – 350 ms, $T_1 = +\infty$ and $B_1 = 0.5 – 1.2$. As shown in the figure, the T_2 estimates obtained from the REPCOM reconstruction increase when the FA decreases from 180° to 120°, while the T_2 maps reconstructed by CURLIE with SEPG fitting (optimized $T_1 = 500$ ms) are comparable for the two different FAs. Note that since the data sets with 180° and 120° FAs were obtained from two separate breath hold acquisitions the slices are similar but not exactly the same.

The T_2 estimates of the phantoms imaged with the liver subject are summarized in Table 3. For both 180° and 120° prescribed FAs, the T_2 estimates by CURLIE with SEPG fitting have < 3.5% error compared to the gold standard T_2. When the effect of indirect echoes is not taken into account in the reconstruction (as in REPCOM), the error can be up to 14% and 38% for FAs of 180° and 120°, respectively. The trend is similar as that shown in Figure 7, and the fact that the T_2 values obtained from CURLIE with SEPG fitting are very similar to the gold standard T_2 values indicates that the CURLIE T_2 maps shown in Figure 7 are accurate.

CURLIE with optimized T_1 SEPG fitting can also be applied for T_2 mapping of the myocardium using data acquired in a single breath hold. In cardiac imaging it is desirable to keep the echo train as short as possible to avoid cardiac motion during data acquisition thus, a short refocusing pulse (i.e., FA< 180°) is typically used. Figure 8, shows the anatomical short-axis cut of the heart acquired with a double-inversion radFSE sequence and T_2 maps reconstructed via CURLIE with SEPG fitting (optimized $T_1 = 700$ ms) and REPCOM. The maps were reconstructed from 16 radial k-space lines per TE (4.0% sampled). Similar to the observation made for the liver, the T_2 maps reconstructed by CURLIE with SEPG fitting are comparable for the two different refocusing pulses, whereas the T_2 maps reconstructed by REPCOM show a greater disagreement between the two refocusing pulses.

Discussion

In this work, we have introduced CURLIE and showed that it can accurately reconstruct the decay curves with indirect echoes from highly undersampled radial MESE data. CURLIE uses a linear approximation of the signal decay allowing for the incorporation of the highly non-linear SEPG model to account for the effects of indirect echoes. Moreover, the TE images generated via CURLIE have high spatial and temporal resolution. As a result, CURLIE combined with SEPG fitting enables accurate T_2 estimation from highly undersampled radial MESE data allowing for the reconstruction of T_2 maps from data acquired in a short period of time. For instance T_2 maps of the whole brain can be achieved in 4 min or less (depending on the degree of undersampling used). Maps of the thoracic cavity and abdomen can be obtained in a breath hold.

As shown in this work, the indirect echoes which are inherent to MESE acquisitions cause a significant (positive) T_2 bias if data are reconstructed assuming an exponential decay. The indirect echo effect is more pronounced for longer T_2s and as the FA of the refocusing pulses deviate from the ideal 180°(17). Thus, without indirect echo compensation, the T_2 estimates from MESE data will depend on the profile of the RF pulse, B_1 imperfections, as well as the TE coverage used in the experiment (number of TE points and echo spacing). As a result, the inter-site or inter-scan reproducibility of T_2 measurements can be greatly impacted. Indirect echoes also limit the use of MESE for T_2 mapping at higher fields (field strength ≥ 3T) where SAR limits the use of 180° refocusing pulses or in cardiac applications where shorter refocusing pulses are used to reduce the acquisition window and minimize the effects of motion.

Our results showed that when curves are reconstructed with CURLIE followed by SEPG fitting the T_2 bias of phantoms (compared to a gold standard) are small and not dependent on the T_2 values and FAs of the refocusing pulses even for data acquired with a high degree of undersampling. The same trend in seen vivo: the T_2 maps of brain, liver and heart reconstructed from highly undersampled data with CURLIE and SEPG fitting are not affected by the prescribed FA of the refocusing pulses as those reconstructed from the REPCOM algorithm. Overall, the technique should provide a fast method for T_2 mapping that is less dependent on the experimental conditions including the magnetic fields strength. These unique characteristics should make the technique practical for clinical use.

In this work SEPG fitting was performed for $T_1 = +\infty$ or an optimized T_1, however, in the reconstruction of the decay curves via CURLIE, T_1 was fixed to infinity. This can be optimized using prior information of the object being imaged and the scanner and imaging parameters. Similar optimization can be performed for the T_2 and B_1 for the generation of the PCs. The T_2 range used to generate the training curves can also be optimized by using prior knowledge based on the anatomy being imaged, or estimated by prior T_2 mapping using a different algorithm (e.g. REPCOM or the echo sharing algorithm described in Ref. 14). In this work we used 6 principal components to approximate the signal model and showed that the T_2 can be accurately estimated in phantoms and a series of in vivo applications such as brain, myocardium and liver. In this work, the number of principal components (L) was determined empirically for the given training set. It is expected that smaller L could yield similar results for an optimized training set. However, given the ranges and/or distributions of T_2, T_1 and B_1, the optimal L and design of the training curves remain open problems.

Although SEPG fitting yields fitted B_1 maps in addition to the T_2 maps, the fitted B_1 maps estimated from our algorithm showed T_1 effects. These manifested as fluctuations along interfaces between tissues with very different T_1s (eg, gray-white matter tissue and CSF or liver parenchyma and blood vessels). However, the nature of the B_1 maps did not affect the T_2 results. We verified this experimentally by comparing the T_2 maps obtained from the CURLIE-SEPG method to those resulting from just SEPG fitting (using standard sampled data when available) or by a using smoothing constraint for the B_1 maps before T_2 estimation. The T_2 maps were similar regardless of the B_1 maps.

For the non-optimized Matlab code used here, the reconstruction took about 40 min using a single core of a desktop computer (Intel Core 2 Quad CPU, 2.4 GHz) for a single slice when the data were acquired with eight coils, 256 k-space lines. However, a significant reduction in reconstruction time is expected when the reconstruction code is optimized and parallelized since most of the computation time was spent on matrix multiplication.

Conclusions

In this work, it has been shown by numerical simulation, phantom and in vivo data that the proposed CURLIE algorithm can accurately reconstruct the decay curves with indirect echoes from highly undersampled radial MESE data. Accurate T_2 estimates can then be derived from the TE curves via SEPG fitting. The use of highly undersampled radial MESE data allows for the fast acquisition of data. The correction for indirect echoes reduces inaccuracies in T_2 mapping due to imperfect refocusing pulses making T_2 mapping with MESE accurate when the FA of the refocusing pulses are less than the ideal 180°; this is particularly important at higher magnetic fields as well as in certain cardiac applications. Overall, the CURLIE algorithm combined with SEPG fitting enables fast T_2 estimation which is less dependent on the experimental conditions used for data acquisition. These improvements should make T_2 mapping more practical for clinical use.

Acknowledgments

This work is sponsored by NIH grant HL085385 (MIA).

References

1. Farraher SW, Jara H, Chang KJ, Ozonoff A, Soto JA. Differentiation of hepatocellular carcinoma and hepatic metastasis from cysts and hemangiomas with calculated T2 relaxation times and the T1/T2 relaxation times ratio. Journal of Magnetic Resonance Imaging. 2006; 24(6):1333–41. [PubMed: 17083093]
2. Cieszanowski A, Szeszkowski W, Golebiowski M, Bielecki DK, Grodzicki M, Pruszynski B. Discrimination of benign from malignant hepatic lesions based on their T2-relaxation times calculated from moderately T2-weighted turbo SE sequence. Eur Radiol. 2002; 12:2273–2279. [PubMed: 12195480]
3. Deng J, Larson AC. Modified PROPELLER Approach for T2-Mapping of the Abdomen. Magnetic Resonance in Medicine. 2009; 61:1269–1278. [PubMed: 19353672]
4. Kim D, Jensen JH, Wu EX, Sheth SS, Brittenham GM. Breathhold Multiecho Fast Spin-Echo Pulse Sequence for Accurate R2 Measurement in the Heart and Liver. Magnetic Resonance in Medicine. 2009; 62:300–306. [PubMed: 19526516]
5. Pell GS, Briellmann RS, Waites AB, Abbott DF, Lewis DP, Jackson GD. Optimized clinical T2 relaxometry with a standard CPMG sequence. Journal of Magnetic Resonance Imaging. 2006; 23:248–252. [PubMed: 16416434]
6. Deoni SCL, Peters TM, Rutt BK. High-resolution T1 and T2 mapping of the brain in a clinically acceptable time with DESPOT1 and DESPOT2. Magnetic Resonance in Medicine. 2005; 53:237–241. [PubMed: 15690526]
7. Rugg-Gunn FJ, Boulby PA, Symms MR, Barker GJ, Duncan JS. Whole-brain T2 mapping demonstrates occult abnormalities in focal epilepsy. Neurology. Jan 25.2005 64:318–325. [PubMed: 15668431]
8. Kurki T, Lundbom N, Valtonen S. Tissue characterisation of intracranial tumours: the value of magnetisation transfer and conventional MRI. Neuroradiology. 1995; 37:515–521. [PubMed: 8570044]
9. Laakso MP, Partanen K, Soininen H, Lehtovirta M, Hallikainen M, Hänninen T, Helkala E-L, Vainio P, Riekkinen PJ Sr. MR T2 relaxometry in Alzheimer's disease and age-associated memory impairment. Neurobiol Aging. 1996; 17:535–540. [PubMed: 8832627]
10. Jacobs MA, Mitsias P, Soltanian-Zadeh H, Santhakumar S, Ghanei A, Hammond R, Peck DJ, Chopp M, Patel S. Multiparametric MRI tissue characterization in clinical stroke with correlation to clinical outcome: part 2. Stroke. 2001; 32:950–957. [PubMed: 11283396]
11. Block KT, Uecker M, Frahm J. Model-Based Iterative Reconstruction for Radial Fast Spin-Echo MRI. IEEE Transactions on Medical Imaging. 2009; (28):1759–1769. [PubMed: 19502124]

12. Huang C, Graff CG, Clarkson EW, Bilgin A, Altbach MI. T2 Mapping from Highly Undersampled Data by REconstruction of Principal COmponent coefficient Maps (REPCOM) using Compressed Sensing. Magnetic Resonance in Medicine. 2012; 67(5):1355–66. [PubMed: 22190358]
13. Doneva M, Sénégas J, Börnert P, Eggers H, Mertins A. Compressed Sensing Reconstruction for Magnetic Resonance Parameter Mapping. Magnetic Resonance in Medicine. 2010; 64(4):1114–1120. [PubMed: 20564599]
14. Altbach MI, Bilgin A, Li Z, Clarkson EW, Trouard TP, Gmitro AF. Processing Of Radial Fast Spin-Echo Data For Obtaining T_2 Estimates From A Single K-Space Data Set. Magnetic Resonance in Medicine. 2005; 54(3):549–559. [PubMed: 16086321]
15. Samsonov, A. A Novel Reconstruction Approach Using Model Consistency Condition for Accelerated Quantitative MRI (MOCCA). Proceedings of the International Society for Magnetic Resonance in Medicine; 2012. p. 358
16. Doneva, M.; Sénégas, J.; Börnert, P.; Eggers, H.; Mertins, A. Accelerated MR Parameter Mapping Using Compressed Sensing With Model-Based Sparsifying Transform. Proceedings of the International Society for Magnetic Resonance in Medicine; 2009. p. 2812
17. Lebel RM, Wilman AH. Transverse Relaxometry with Stimulated Echo Compensation. Magnetic Resonance in Medicine. 2010; 64:1005–1014. [PubMed: 20564587]
18. Poon CS, Henkelman RM. Practical T2 quantitation for clinical applications. Journal of Magnetic Resonance Imaging. 1992; 2:541–553. [PubMed: 1392247]
19. Majumdar S, Orphanoudakis SC, Gmitro A, O'Donnell M, Gore JC. Errors in the measurements of T2 using multiple-echo MRI techniques.I. Effects of radiofrequency pulse imperfections. Magnetic Resonance in Medicine. 1986; 3:397–417. [PubMed: 3724419]
20. Does MD, Snyder RE. Multiecho imaging with suboptimal spoiler gradients. Journal of Magnetic Resonance Imaging. 1998; 131:25–31.
21. Hennig J. Multiecho Imaging Sequences with Low Refocusing Flip Angles. Journal of Magnetic Resonance. 1988; 78:397–407.
22. Huang, C.; Bilgin, A.; Graff, C.; Altbach, MI. T2 Estimation For Small Lesions Using A Model-Based Reconstruction With Sparsifying Penalty Functions And Highly Undersampled Radial FSE Data. Proceedings of the International Society for Magnetic Resonance in Medicine; 2009. p. 2740
23. Sénégas, J.; Neu, N.; Keupp, J. Transverse Relaxometry with non-180° Refocusing Pulses. Proceedings of the International Society for Magnetic Resonance in Medicine; 2011. p. 2761
24. Altbach MI, Outwater EK, Trouard TP, Krupinski, Elizabeth A, Theilmann RJ, Stopeck AT, Kono M, Gmitro AF. Radial fast spin-echo method for T2-weighted imaging and T2 mapping of the liver. Journal of magnetic resonance imaging: Journal of Magnetic Resonance Imaging. 2002; 16(2):179–189.
25. Theilmann RJ, Gmitro AF, Altbach MI, Trouard TP. View-ordering in radial fast spin-echo imaging. Magnetic Resonance in Medicine. 2004; 51(4):768–774. [PubMed: 15065250]
26. Haacke, EM.; Brown, RW.; Thompson, MR.; Venkatesan, R. Magnetic Resonance Imaging: Physical Principles and Sequence Design. Wiley; 1999.
27. Simonetti OP, Finn JP, White RD, Laub G, Henry DA. Black blood T2-weighted inversion recovery MR imaging of the heart. Radiology. 1996; (199):49–57. [PubMed: 8633172]
28. Polak E, Ribiere G. Note sur la Convergence des Méthodes de Directions Conjuguées. Revue Française d'Informatique et de Recherche Opérationelle. 1969; 16:35–43.
29. Deoni SC, Rutt BK, Peters RM. Rapid Combined T1 and T2 Mapping Using Gradient Recalled Acquisition in the Steady State. Magnetic Resonance in Medicine. 2003; 49:515–526. [PubMed: 12594755]
30. Wood ML, Bronskill MJ, Mulkern RV, Santyr GE. Physical MR desktop data. J Magn Reson Imaging. 1993; (3 Suppl)
31. Ratner AV, Okada RD, Newell JB, Pohost GM. The relationship between proton nuclear magnetic resonance relaxation parameters and myocardial perfusion with acute coronary arterial occlusion and reperfusion. Circulation. 1985; 71:823–828. [PubMed: 3971547]

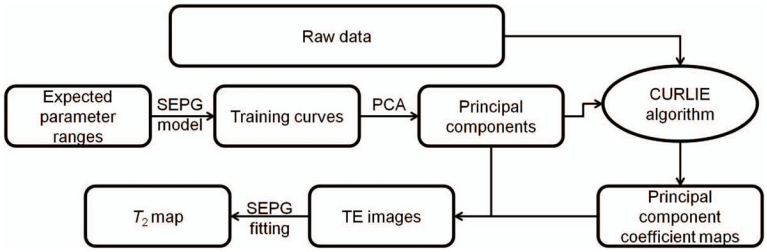

Figure 1.
Flow chart depicting the CURLIE-SEPG fitting algorithm.

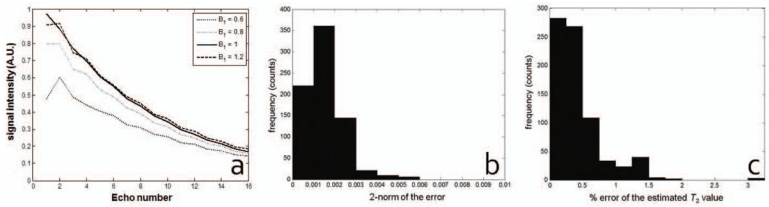

Figure 2.

(a) Selected training curves for T_2 = 100 ms, T_1 = + ∞ and B_1 ranging from 0.6 to 1.2. Curves were simulated numerically using the SEPG model. An echo spacing of 12.11 ms was used in the simualtions to cover a TE range similar to in vivo data. (b) The distribution of the 2-norms of the approximation error for training curves generated according to the SEPG model using only 6 PCs; (c) The distribution of the % error of the T_2 values caused by the approximation error when 6 PCs are used to represent the training decay curves. Note that the 2-norms of the approximation error are all below 0.006 and the % error of the T_2 values are all less than 3.5% which indicates that the curves are well represented with only 6 PCs.

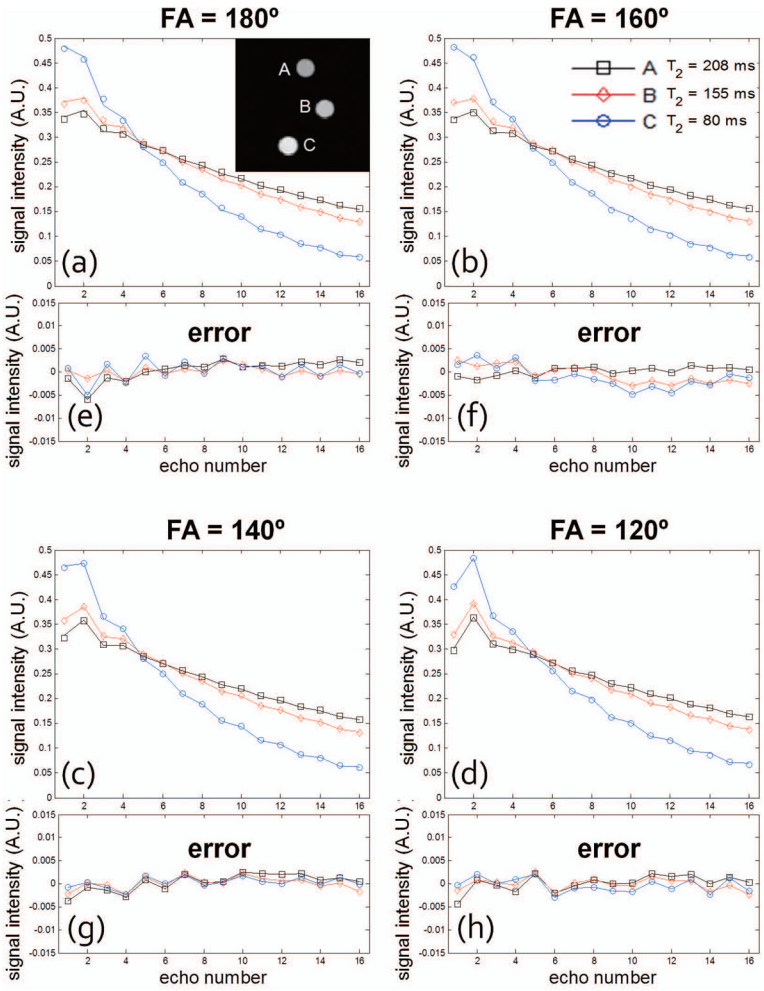

Figure 3.

(a–d) Decay curves for each of the three tubes in the phantom for different refocusing FA obtained from a standard sampled radial MESE data set (i.e. 256 radial views with 256 points per view). Data were acquired with echo spacing of 12.11 ms to mimic the TE coverage in vivo. Each point in the decay curves corresponds to the averaged signal from voxels within an ROI for each tube; each curve is the fitted curve according to the SEPG model. The curves are normalized (2-norm=1). (e–h) The approximation error when 6 PCs are used to represent the decay curves. Note that the errors are all below 0.01 (with most under 0.005) for all FAs which show that 6 PCs can represent the decay curves of the acquired data well.

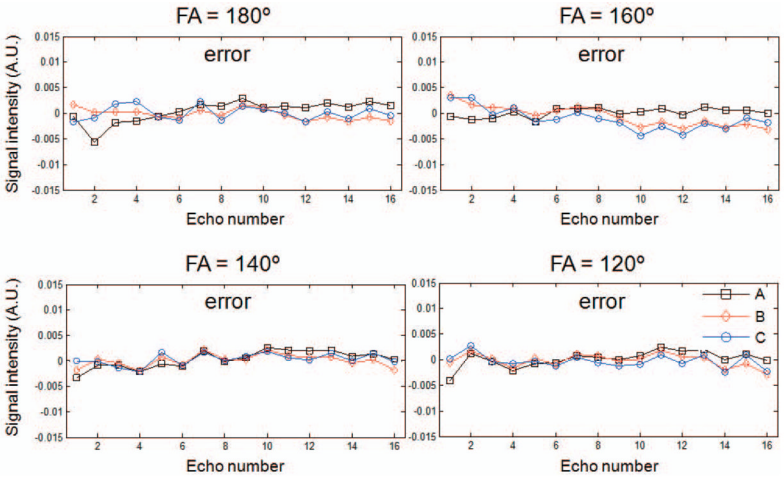

Figure 4.

The errors of the decay curves of the three-tube phantom shown in Figure 3 reconstructed from highly undersampled radial MESE data (4% sampled relative to the Nyquist condition) by using the CURLIE algorithm. Data were acquired with echo spacing of 12.11 ms to mimic the TE coverage in vivo. Note that the differences between the curves are small (the 2-norms of the differences are between 0.0035 and 0.0095) which demonstrates that decay curves from highly undersampled data can be accurately reconstructed with the CURLIE algorithm.

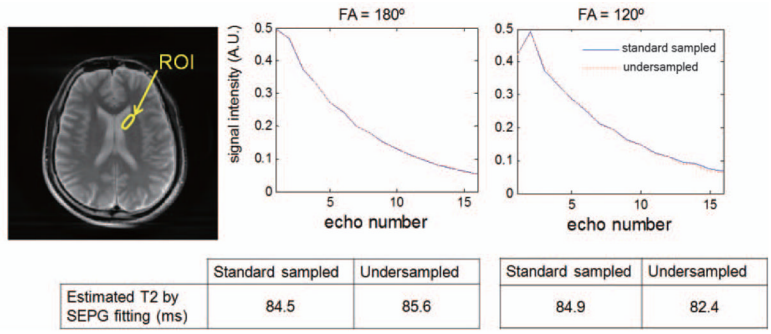

	Standard sampled	Undersampled
Estimated T2 by SEPG fitting (ms)	84.5	85.6

Standard sampled	Undersampled
84.9	82.4

Figure 5.

Decay curves of the ROI obtained from standard sampled and 8 times less sampled radial MESE data acquired with FAs of the refocusing pulses prescribed to 180° and 120°. The T_2 values for standard sampled data were obtained directly from the reconstructed TE images using SEPG fitting. The T_2 values for undersampled data were obtained using CURLIE followed by SEPG fitting. $T_1 = +\infty$ was used for the SEPG fitting. Data were acquired with echo spacing = 12.93 ms. Note that the curves generated from undersampled data via CURLIE are similar to the standard sampled curves (obtained directly from the acquired data). The differences between the T_2 values obtained from under- and standard sampled data are below 3%. Also, the T_2 values estimated from data acquired with 180° and 120° FAs are similar.

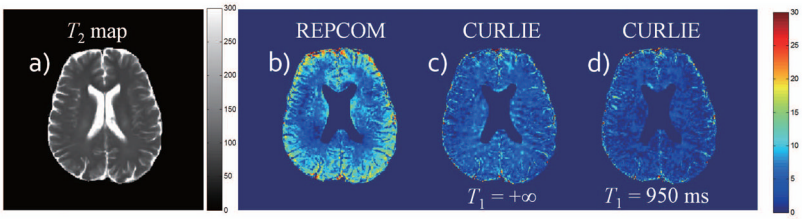

Figure 6.

(a) Voxel-wise T_2 map obtained by CURLIE and SEPG fitting (T_1=950 ms) from the data acquired with the FAs of the refocusing pulses prescribed to 180°. (b–d) The %difference between T_2 maps obtained from data acquired with prescribed FAs of 180° and 120° using REPCOM (which ignores indirect echoes) and CURLIE with SEPG fitting. Each difference map was obtained from the T_2 maps obtained by the same fitting algorithm for the prescribed FAs of 180° and 120°. The difference maps support the concept that the CURLIE reconstruction followed by SEPG fitting significantly reduces the effect of indirect echoes in T_2 estimation.

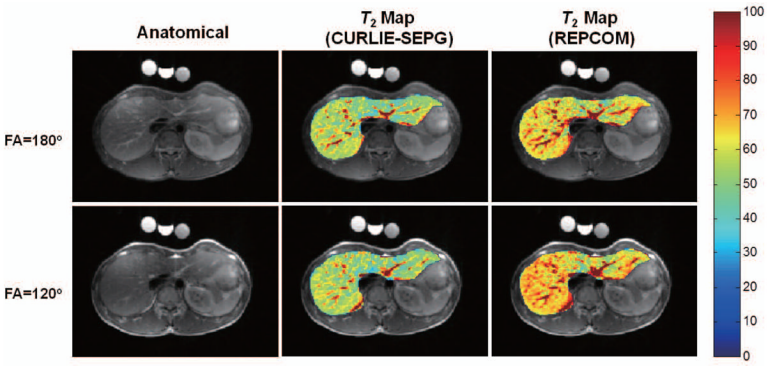

Figure 7.

(left) Anatomical abdominal images reconstructed from the same data used for T_2 map generation. (middle) Liver T_2 maps (overlaid onto the anatomical image) obtained by CURLIE and SEPG fitting (T_1 = 500 ms) from undersampled data acquired with two refocusing pulses (FA=180° and 120°). (right) The T_2 maps reconstructed by REPCOM (which ignores indirect echoes) using the same undersampled data sets as in the CURLIE reconstruction. Note that the T_2 estimates obtained from the REPCOM reconstruction increase when the FA decreases from 180° to 120°, while the T_2 maps reconstructed by CURLIE with SEPG fitting are comparable for the two different FAs.

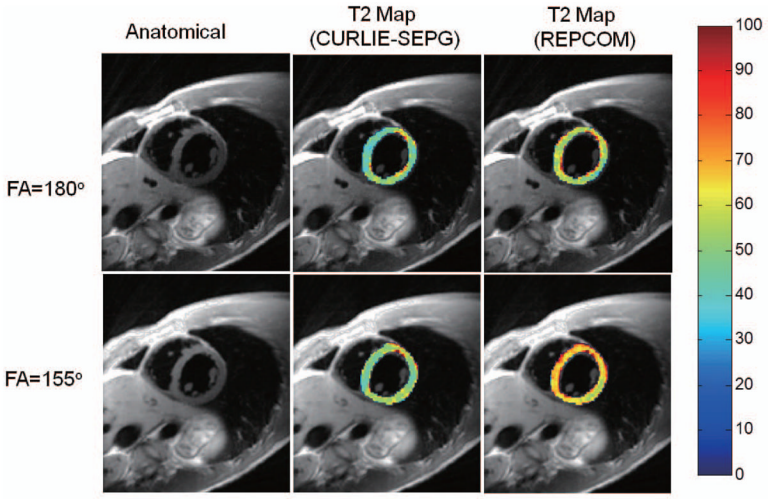

Figure 8.

(left) Anatomical cardiac images reconstructed from the same data used for T_2 map generation. (middle) T_2 maps of the left ventricular heart wall (overlaid onto the anatomical image) obtained by CURLIE and SEPG fitting (T_1 = 700 ms) from undersampled data for normal refocusing pulses (FA =180°) and the short-duration refocusing pulses (FA =155°). (right) The T_2 maps reconstructed by REPCOM (which ignores indirect echoes) using the same undersampled data sets as in the CURLIE reconstruction. T_2 maps reconstructed by CURLIE with SEPG fitting are comparable for the two different refocusing pulses, whereas the T_2 maps reconstructed by REPCOM show a greater disagreement between the two refocusing pulses.

Table 1

Percent error of T_2 estimates (relative to the gold standard) for the of the physical phantom shown in Figure 3. The table shows % error of T_2 values estimated from curves derived directly from the TE images (original curves) and curves recovered from the first 6 PCs. Results shown are for standard sampled radial data (i.e., data for each TE time point has 256 radial lines with 256 points per line).

Exponential Fitting						
	Vial	**Gold standard**	**FA=180**	**FA=160**	**FA=140**	**FA=120**
Original curves	A	**210.0**	5.7%	5.7%	9.6%	18.3%
	B	**159.3**	3.6%	2.8%	5.9%	13.4%
	C	**80.7**	3.2%	2.1%	5.0%	12.0%
Recovered curves	A	**210.0**	5.6%	5.7%	9.8%	18.4%
	B	**159.3**	3.6%	2.7%	6.0%	13.6%
	C	**80.7**	3.1%	1.9%	5.0%	12.0%

SEPG fitting with T_1=+∞						
	Vial	**Gold standard**	**FA=180**	**FA=160**	**FA=140**	**FA=120**
Original curves	A	**210.0**	0.7%	−0.9%	−2.0%	−3.7%
	B	**159.3**	−1.2%	−3.0%	−4.0%	−5.5%
	C	**80.7**	−0.5%	−2.9%	−4.2%	−5.8%
Recovered curves	A	**210.0**	0.8%	−0.9%	−1.9%	−3.8%
	B	**159.3**	−1.2%	−3.0%	−4.0%	−5.6%
	C	**80.7**	−0.6%	−2.9%	−4.2%	−5.8%

SEPG fitting with T_1 optimized (500 ms)						
	Vial	**Gold standard**	**FA=180**	**FA=160**	**FA=140**	**FA=120**
Original curves	A	**210.0**	2.4%	1.2%	1.8%	3.2%
	B	**159.3**	0.0%	−1.6%	−1.6%	−0.8%
	C	**80.7**	−0.4%	−2.5%	−3.2%	−3.6%
Recovered curves	A	**210.0**	2.4%	1.2%	1.8%	3.1%
	B	**159.3**	0.0%	−1.6%	−1.6%	−0.9%
	C	**80.7**	−0.4%	−2.5%	−3.2%	−3.6%

Table 2

Percent error of T_2 estimates (relative to the gold standard) for highly undersampled data (4% sampled compared to fully sampled radial data). Data shown corresponds to the vials of the physical phantom shown in Figure 2. T_2 estimation was performed using CURLIE for the generation of curves followed by SEPG fitting with $T_1 = +\infty$.

Fitting algorithm	Vial	Gold standard	FA=180	FA=160	FA=140	FA=120
SEPG fitting with T_1=+∞	A	**210.0**	−0.9%	−2.1%	−3.5%	−4.0%
	B	**159.3**	0.3%	−0.9%	−4.0%	−4.7%
	C	**80.7**	0.5%	−0.4%	−4.6%	−4.8%
SEPG fitting with T_1=500 ms	A	**210.0**	1.0%	−0.1%	−0.2%	2.3%
	B	**159.3**	1.6%	0.5%	−1.8%	−0.1%
	C	**80.7**	0.6%	0.0%	−4.0%	−2.7%

Table 3

Percent error of T_2 estimates (relative to the gold standard) for the phantoms acquired with the liver data shown in Figure 7. T_2 curves were reconstructed from undersampled data (4% sampled) using CURLIE or the REPCOM algorithm (which does not compensate for indirect echoes). T_2 estimates from the CURLIE curves were obtained by SEPG fitting with "optimized" T_1 (500 ms). T_2 estimates from REPCOM were obtained using an exponential fit to the data.

	Gold Standard (ms)	FA = 180°		FA = 120°	
		CURLIE+SEPG	REPCOM	CURLIE+SEPG	REPCOM
a	53.2	−2.3%	6.4%	−3.2%	20.7%
b	77.9	1.0%	14.4%	3.1%	38.9%
c	64.0	−2.0%	12.0%	−1.3%	36.4%